Mission-oriented Modular Control of Retrofittable Marine Power Plants

Ir. M.C. van Benten[a]*, N. Kougiatsos MSc[a], Dr. V. Reppa[a]

[a]*Maritime and Transport Technology, Faculty of Mechanical, Maritime and Materials Engineering, Delft University of Technology, 2628CD, the Netherlands*
*Corresponding author. Email: M.C.vanBenten@tudelft.nl

Synopsis

This paper presents the design methodology of a mission-oriented modular control system for marine power plants. To this end, first power profiles, power plant layouts and control systems of multiple vessels such as tugboats, offshore support vessels, cargo ships and cruise ships are analyzed. By decomposing the power profile in two components, the propulsion and auxiliary power demand, the correlation between the power profile of a vessel and its mission is derived, and an algorithm that computes the power profile using mission and vessel data is proposed. Furthermore, the correlation between the power profile and the layout of the power plant is also investigated, with emphasis on how changes in the power profile result in power plant automation modifications. A modular secondary control level is then designed to cope with the required power plant automation modifications, by combining the Equivalent Consumption Minimization Strategy (ECMS) with Supervisory Switching Control (SSC). In this paper we consider battery modifications, following the example of Wärtsilä's ZESPacks. Simulation results are used to show the performance of the proposed switching control methodology, in relation to the stability of the components in the power plant after automation modifications occur. The main contribution of this paper is the novel approach for the secondary level power plant control system, introducing modularity to the otherwise assumed fixed layout of the power plant. Furthermore, the proposed algorithm can be used to determine the expected power profile for a new mission, and to identify required modifications of the power plant equipment.

Keywords: Marine control systems, Modular control architecture, Hybrid power plant, Battery modifications

1 Introduction

Marine vessels are used for shipping cargo, (supporting) offshore operations, transporting passengers, or even to tow other marine vessels. During their lifetime they execute many missions, and each mission requires power, either for propulsion or for other tasks (e.g. air conditioning, electric load for on-board systems, boilers). The power required during a mission is used to construct the power profile, and is generated by the power plant. How the power plant is designed is partly based on the expected missions the vessel will execute (Hanbidge, 2001), resulting in a fixed power plant, and therefore a fixed control system. However, each mission results in a different power profile, since there are different environmental conditions (such as wind, waves and currents) and operational conditions (e.g. the frequency of the required actions of the vessel, such as loading or unloading cargo, sail across open sea or towing another vessel). Therefore, each mission implies a certain required amount of equipment in the power plant. By using a fixed set of equipment, this could result in situations where the power plant is not sufficient for generating the power demand dictated by a new mission, which may lead to inefficient use of the power plant components, risk of overloading the components, or even the inability to execute the mission properly. To handle this issue, equipment modification such as additions, removals, or replacements would probably be necessary, along with modifications of the control architecture.

In literature, many different power plants can be found, and they can be classified as mechanical, electric, or hybrid. In this paper, a hybrid power plant is considered, of which an example is shown in Figure 1. The control system of the power plant is part of the marine control system, and the latter is deployed in a hierarchical, distributed architecture. This general control architecture can be divided into three levels (Geertsma et al., 2017a; Smogeli et al., 2005; Smogeli, 2006; Smogeli et al., 2008; Smogeli and Sørensen, 2009):

Authors' Biographies

Ir. Marcel van Benten is currently a PhD researcher at Delft University of Technology. He recently graduated on the topic of this paper, and is now researching the storage, bunkering and handling of solid hydrogen carriers.

Nikos Kougiatsos MSc is currently a PhD researcher at Delft University of Technology. His research involves scalable, modular control and fault-tolerant control strategies for marine vessels. During his Master's in Naval Architecture and Marine Engineering, he has been awarded scholarships from the American Bureau of Shipping (ABS).

Dr. Vasso Reppa is an Assistant Professor with the Transport Engineering and Logistics Section of the Maritime and Trans- port Technology Department, Delft University of Technology. Dr. Reppa's research interests include fault tolerant control, fault diagnosis, interconnected uncertain systems, multi-agent control, autonomous shipping operations and waterborne transport.
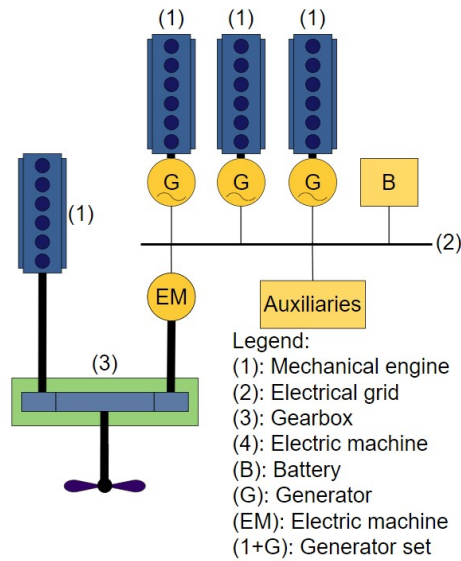
Figure 1: Example of a hybrid power plant (constructed using the figures of Geertsma et al. (2017a))
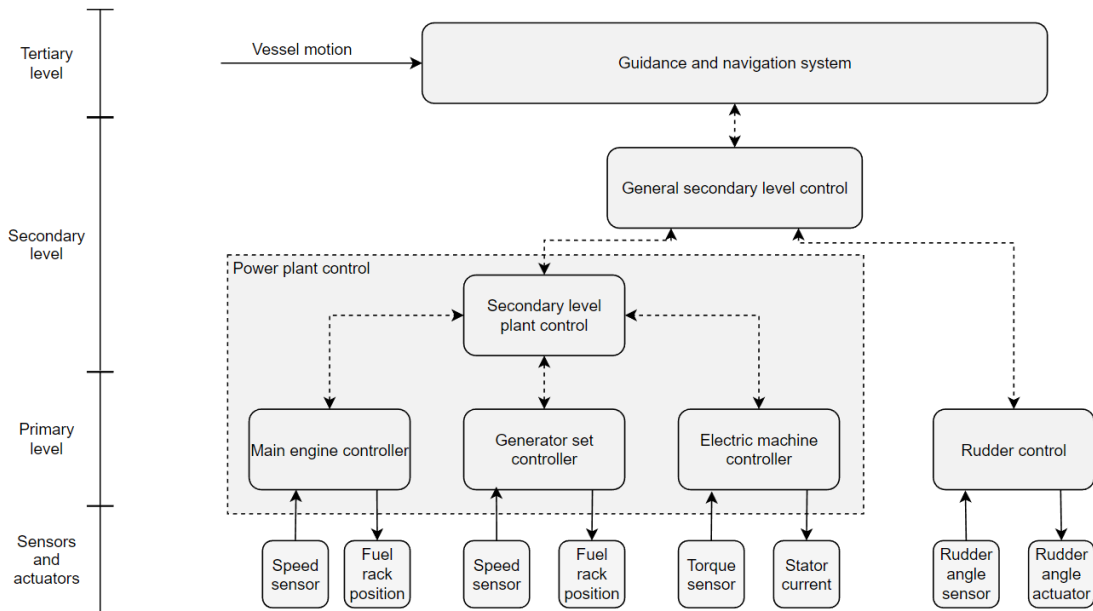

Figure 2: Multi-level marine vessel control system (Van Benten, 2021)

- Local optimizer/tertiary level

- Secondary level

- Primary level

The local optimizer is also known as the guidance and navigation system, and the main task of this system is to determine the desired path for the ship, and to provide the reference signals for the general secondary level control that includes a path-following controller (Wang et al., 2018). The secondary level plant control determines the distribution of power to the components in the power plant, from now on this will be referred to as the power split. Based on the defined power split the set-points for the primary level control are generated. The primary level consists of the controllers of all the components in the power plant (Geertsma et al., 2017a). The control operation of the hybrid power plant in Figure 1 can be deployed in a multi-level control architecture, as shown in Figure 2. As each vessel is designed with a certain power plant layout, the multi-level control system of Figure 2 is designed to control a specific set of power plant equipment, and often Equivalent Consumption Minimization Strategy (ECMS) is used in the secondary level plant control. This strategy requires a cost function that expresses

the power of each component in terms of fuel use, and determines the power split by minimizing the cost function at each instance, while meeting several constraints that limit the power of each component and ensure that the power demand is met. However, it is seen in literature that vessels often have a fixed power plant, and a fixed control system (Van Benten, 2021), although their missions lead to different power requirements. This could introduce inefficient use, or overloading of the power plant equipment, or even the inability to carry out future missions. Let us consider three examples of diesel-electric tugboats found in (Vu et al., 2015; Yuan et al., 2016; Kumar et al., 2020). Although their operations are alike, the power profile differs, as shown in Figure 3, where the propulsion power P_D is shown, and it can also be noted that the installed equipment is different.
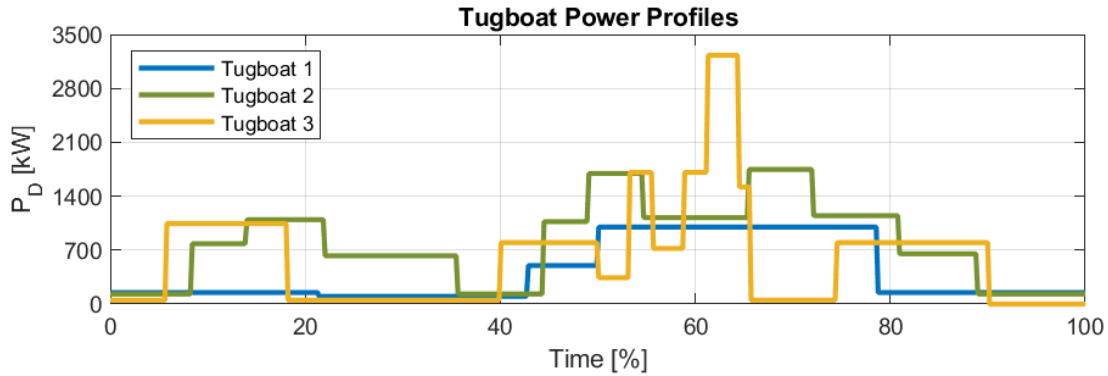

Figure 3: Comparison of different tugboats (Vu et al., 2015; Yuan et al., 2016; Kumar et al., 2020)

By comparing the power profiles and the power plants of the corresponding tugboats, it is noted that for missions with more power demand, the capacity of the generator sets and the batteries should increase. If for example tugboat 1 has to carry out the mission of tugboat 2, both a generator set and a battery has to be added or replaced. Vice versa, tugboat 2 could execute the mission associated with tugboat 1 with less equipment, reducing the weight of the ship. Thus, the equipment modifications that might be needed in the system architecture can be classified as:

- Additions of components

- Replacements of components

- Removals of components

The state-of-the-art power plant control systems consist of two levels: a secondary level to compute the power split and reference signals, and a primary level that controls the equipment in the power plant, using the derived reference signals. These two levels depend on the current layout of the power plant. Therefore, if equipment is added or removed, the layout definitely changes, but also for replacements, the characteristics of the equipment may change. Hence for all equipment modifications the control system needs to be updated. To be able to automate this process, a control system that can determine the required equipment modifications based on the power profile is proposed, and described next. It would be beneficial to facilitate automation modifications of the power plant of the vessel during missions. The current practice though in state-of-the-art automatic control of marine vessels is that the control system has to be manually tuned to be able to control the new power plant. Furthermore, from the perspective of the control system, multiple batteries in a power plant are considered as a single battery (Kalikatzarakis et al., 2018), which does not contribute to the modularity. To this end, this paper presents a design of a modular control system for a retrofittable power plant, allowing modular use of the power plant equipment without the need to manually tune the control system.

In this work, in order to design a control system for a retrofittable power plant, first the correlation between the mission and the power profile of the vessel is needed, in order to find the impact of varying missions on the power demand during missions. Then, a decision logic is designed to map the changes in the power profile to the changes in the power plant. Using this, a modular power plant architecture is proposed to meet these automation modifications. At last, the designed architecture is verified, with respect to stability and robustness.

This paper is structured as follows. In Section 2 the problem formulation is presented, discussing the design of the power plant and control system. In Section 3 a model for the correlation between the mission and the power profile along with the correlation between the power profile and the needed automation modifications in the control system and power plant are discussed. In Section 4 the design of a modular control architecture is proposed, aiming to meet the required automation modifications. In Section 5 the performance of the proposed design is verified, showing the stability and robustness of the modular control architecture. At last, in Section 6 some concluding remarks are provided.

2 Problem formulation

Let us consider the hybrid power plant shown in Figure 4. For propulsion, a parallel control strategy is deployed (Geertsma et al., 2017c). The operation of each component is described as follows:

2.1 Diesel engine

The dynamic operation of the diesel engine is expressed as a first-order differential equation (Haseltalab and Negenborn, 2019):

$$\dot{Q}_{DE}(t) = -\frac{Q_{DE}(t)}{\tau_{DE}(t)} + k_{DE} \cdot m_{f,DE}(t) \tag{1}$$

where Q_{DE} is the torque of the diesel engine, k_{DE} is the torque constant, $m_{f,DE}$ is the fuel index (regulated by a PI controller), and τ_{DE} is the torque buildup constant which determines the response speed of the diesel engine, as a function of the shaft speed ω_{DE}:

$$\tau_{DE}(t) = \frac{0.9}{\omega_{DE}(t)} \tag{2}$$

2.2 Induction motor

The operation of the induction motor can be described as (Eijkhout and Jovanova, 2021; Wildi et al., 2002):

$$Q_{IM}(t) = \frac{\omega_{IM,s}(t) - \omega_{IM}(t)}{\omega_{IM,s}(t)} \cdot \frac{V_{IM}^2(t)}{R_{r,IM} \cdot k_{IM}} \tag{3}$$

where Q_{IM} is the generated torque, ω_{IM} is the rotor speed, $\omega_{IM,s}$ is the rotational speed of the magnetic field in the stator windings, also referred to as the stator speed, V_{IM} is the input voltage (in literature often referred to as phase voltage), $R_{r,IM}$ is the rotor resistance, and k_{IM} is a constant that depends on the motor characteristics. As $\omega_{IM,s}$ is regulated by a PI controller, the input voltage V_{IM} is proportional to $\omega_{IM,s}$ (Vahedpour et al., 2015):

$$V_{IM}(t) = C_{V/f} \cdot \omega_{IM,s}(t) \tag{4}$$

where $C_{V/f}$ is a motor dependent constant.

2.3 Gearbox, shaft, and propeller

The shaft dynamics of the gearbox, shaft and propeller, are expressed as (Woud and Stapersma, 2019; Haseltalab and Negenborn, 2019; Geertsma et al., 2017b, 2016; Geertsma, 2019):

$$\dot{\omega}_p(t) = \frac{\eta_T(i_{DE} \cdot Q_{DE}(t) + i_{IM} \cdot Q_{IM}(t)) - Q_p(t)}{J_{tot}} \tag{5}$$

where ω_p is the propeller speed, Q_p is the propeller torque, J_{tot} is the total inertia of the gearbox, induction machine and the diesel engine together, i_{DE} and i_{IM} the gear ratios of the diesel engine and the induction motor, respectively, and η_T is the transmission efficiency. The propeller torque Q_p is defined as (Izadi-Zamanabadi and Blanke, 1999; Smogeli, 2006):

$$Q_p(t) = C_p \cdot |\omega_p(t)| \cdot \omega_p(t) \tag{6}$$

where C_p is the propeller constant. Since the diesel engine, the induction machine, and the propeller are rigidly coupled, ω_{DE} and ω_{IM} can be expressed in terms of ω_p:

$$\omega_{IM}(t) = i_{IM} \cdot \omega_p(t) \tag{7}$$
$$\omega_{DE}(t) = i_{DE} \cdot \omega_p(t) \tag{8}$$

2.4 Diesel generator sets

The engine of the diesel generator set is modeled as follows (Haseltalab and Negenborn, 2019):

$$\dot{Q}_{DG,DE}(t) = -\frac{Q_{DG,DE}(t)}{\tau_{DG}(t)} + k_{DG} \cdot m_{f,DG}(t) \tag{9}$$

where $Q_{DG,DE}$ is the torque of the diesel engine connected to the generator, k_{DG} the torque constant, $m_{f,DG}$ the fuel index (regulated by a PI controller), and τ_{DG} is the torque buildup constant which determines the response speed of the diesel engine, as a function of the shaft speed ω_{DG}:

$$\tau_{DG}(t) = \frac{0.9}{\omega_{DG}(t)} \tag{10}$$

The dynamics of the generator are described with a set of algebraic equations (Cheong et al., 2010):

$$Q_{DG,G}(t) = \frac{(a_{G,1} \cdot I_X(t) + a_{G,0}) \cdot Re(I_{DG}(t))}{2\pi} \tag{11}$$

$$I_{DG}(t) = \frac{(a_{G,1} \cdot I_X(t) + a_{G,0}) \cdot \omega_{DG}(t)}{2\pi(R_{DG,int} + j \cdot L_{DG} \cdot \omega_{DG}(t) + R_{DG}(t))} \tag{12}$$

$$\dot{\omega}_{DG}(t) = \frac{Q_{DG,DE}(t) - Q_{DG,G}(t)}{J_{DG}} \tag{13}$$

where $Q_{DG,G}$ is the generator torque, I_X the excitation current, $a_{G,1}$ and $a_{G,0}$ are constants, I_{DG} the generator output current, $R_{DG,int}$ the internal resistance, L the inductance, j the imaginary number, and J_{DG} the generator inertia. In this work the load resistance R_{DG} is assumed to be purely resistive, and determined with the assigned power P_{DG} and the reference-voltage $V_{DG,ref}$ as follows:

$$R_{DG}(t) = \frac{V_{DG,ref}^2(t)}{P_{DG}(t)} \tag{14}$$

2.5 Batteries and constraint modules

Batteries can be described with a set of algebraic equations (Sun and Shu, 2011; Kularatna and Gunawardane, 2021; Chang, 2013; Haseltalab et al., 2020):

$$P_B(t) = V_B(t) \cdot I_B(t) \tag{15}$$
$$V_B(t) = V_{OC}(t) - R_B \cdot I_B(t) \tag{16}$$
$$V_{OC}(t) = a_{B,1} \cdot SOC(t) + a_{B,0} \tag{17}$$
$$SOC(t) = SOC(t_0) - \frac{1}{C_0} \int_{t=0}^{t} I_B(t)dt \tag{18}$$

where P_B and I_B are the battery power and the battery current, respectively (both positive for discharging), V_B the battery output voltage, V_{OC} the open-circuit voltage, $a_{B,0}$ and $a_{B,1}$ are constants, C_0 the capacity, and $SOC(t_0)$ the initial SOC. The main goal of the constraint module is to provide a window $[P_B^{min} \quad P_B^{max}]$ for P_B to the secondary level, such that the SOC and V_B are kept within their predescribed limits. Based on the work of (Kalikatzarakis et al., 2018) this leads to the following constraints:

$$P_{B,V}^{max} = \frac{V_{OC} \cdot V_{B,min} - V_{B,min}^2}{R_B} \tag{19}$$

$$P_{B,V}^{min} = \frac{V_{B,max}^2 - V_{OC} \cdot V_{B,max}}{R_B} \tag{20}$$

$$P_{B,SOC}^{max} = \frac{SOC - SOC_{min}}{\Delta t} \cdot C_0 \cdot V_{OC} \tag{21}$$

$$P_{B,SOC}^{min} = \frac{SOC - SOC_{max}}{\Delta t} \cdot C_0 \cdot V_{OC} \tag{22}$$

$$P_B^{min} = max\left(P_{B,SOC}^{min}, P_{B,V}^{min}\right) \tag{23}$$
$$P_B^{max} = min\left(P_{B,SOC}^{max}, P_{B,V}^{max}\right) \tag{24}$$

where $V_{B,min}$, $V_{B,max}$, SOC_{min}, and SOC_{max} are the minimum and maximum terminal voltage V_B and minimum and maximum SOC of the battery, respectively, provided by the battery manufacturer, and Δt is a discrete timestep, which can be tuned to alter the power constraints related to the SOC of the battery.

The objective of this work is to design a modular control architecture that can facilitate the addition, replacement, or removal of batteries, to satisfy a power profile that changes with respect to the mission of the marine vessel.
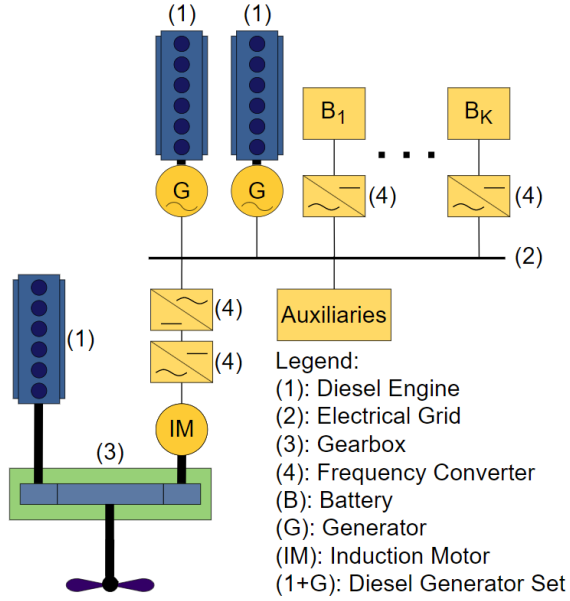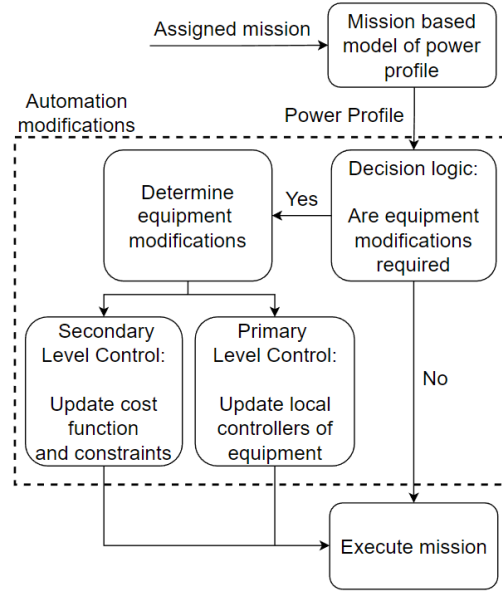
Figure 4: Modular power plant layout

Figure 5: Correlation between the mission, power profile and the automation modifications

3 Correlation between the mission, power profile, and the required automation modifications

The correlation between the mission, the power profile, and the required automation modifications is discussed in this section and is depicted in Figure 5.

3.1 Mission and power profile

There is no consensus of a general definition of mission, hence we propose the following mission definition:

"Transport X from A to B (optionally via C, D, etc.), leaving at t_0 (time and date), arriving at destination at t_{end} (time and date)."
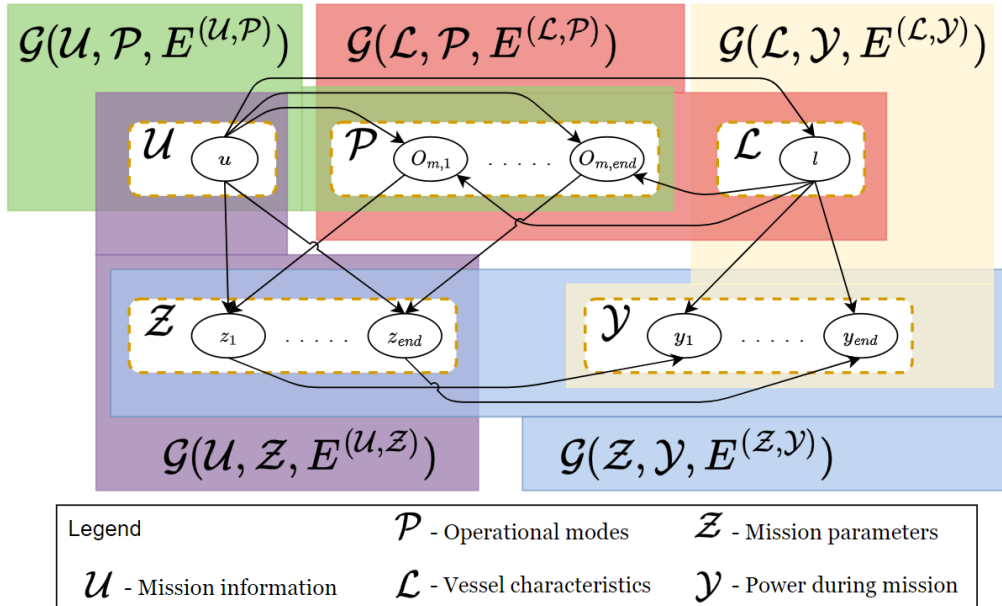
Figure 6: Mission based model of power profile. The set of mission information is expressed as u, the set of vessel characteristics as l, the set of mission parameters as z, and the set of power during the mission as y. Also, an index $i \in [1, ..., end]$ is used to illustrate time-dependency. The notation $\mathcal{G}(\mathcal{I}, \mathcal{O}, E^{(\mathcal{I},\mathcal{O})})$ denotes the graph between the sets $\mathcal{I}$ and $\mathcal{O}$ with vertices $E^{(\mathcal{I},\mathcal{O})}$ (depicted as arrows), the latter showing the relation between the sets. Finally, each distinct graph is enclosed by a different color

where X denotes the cargo/passengers/vessel in need of transportation, and $A \in R^2$ and $B \in R^2$ are the coordinates (latitude and longitude) of the locations visited.

Following the approach presented in (Milis et al., 2017), the correlation between the mission, power profile, and the different aspects can be seen in Figure 6. Using the mission definition and the notation seen in the graph-model, the input $\mathcal{U}$ is defined as $\{A, B, t_0, t_{end}, X\}$, and with this input three sets with information required to construct the power profile can be derived. The first set describes the vessel characteristics $\mathcal{L} = \{X_v, a, D, f_h, K_Q, K_T, \eta_D\}$, and contains the type of vessel X_v, and vessel characteristics such as the proportionality between the vessel speed and required power a, propeller diameter D, fouling f_h, torque coefficient K_Q, thrust coefficient K_T, and propulsive efficiency η_D. The second set contains the required operational mode (O_m) for each point $i \in [1,...,end]$ during the mission, denoted as $\mathcal{P} = \{O_{m,1}, ..., O_{m,end}\}$. At last, the required mission parameters are captured in $\mathcal{Z} = \{z_1, ..., z_{end}\}$, with z_i for $i \in [1,...,end]$ the set of parameters at point i in the mission, such as travelled route S_m, the environmental conditions O_e (waves w_s, currents c_s, wind w_w, ambient temperature T_a, water depth h, and waterway width w_w) along the route, the speed of the vessel during each operational mode V_{O_m}, and also details such as the displacement ∇, and the towing force F_{tow} during the mode *assist*, if applicable. These aspects determine the power required during the mission, hence they determine the output $\mathcal{Y} = \{y_1,...,y_{end}\}$ with $y_i = \{P_{D,i}, P_{aux,i}, P_{tot,i}\}$, where P_D is the propulsion power, P_{aux} is the auxiliary power, and $P_{tot} = P_D + P_{aux}$ is the total power.

Now, using a mission with two locations (A and B) to be visited, cargo X, starting time t_0 and total mission time $t_m = t_{end} - t_0$, an algorithm that determines the required power profile for a given mission can be proposed, as shown in Algorithm 1. For a more detailed description of this algorithm and e.g. the functions $f_{\mathcal{L}}$, $f_{\mathcal{P}}$, $f_{\mathcal{Z}}$, and $f_{\mathcal{Y}}$ the reader is referred to (Van Benten, 2022).

Algorithm 1: Correlation between mission and power profile

Input: $\mathcal{U} = \{A, B, t_0, t_{end}, X\} \leftarrow$ Derived from mission definition or historical data

---

1 $\mathcal{L} = f_{\mathcal{L}}(\mathcal{U}) = \{X_v, a, D, f_h, K_Q, K_T, \eta_D\} \leftarrow$ Vessel characteristics
2 $\mathcal{P} = f_{\mathcal{P}}(\mathcal{U}, \mathcal{L}) = \{O_{m,1}, ..., O_{m,end}\}$ $\leftarrow$ Operational modes
3 $O_{e,i} = \{s_{s,i}, c_{s,i}, w_{s,i}, h_i, T_{a,i}, w_{w,i}\}$ $\leftarrow$ Operational environment
4 $z_i = \{ S_{m,i}, F_{tow,i}, O_{e,i}, \nabla_i, V_{O_{m,i}}, c_{0,i}\}$ $\leftarrow$ Mission parameters
5 $\mathcal{Z} = f_{\mathcal{Z}}(\mathcal{U}, \mathcal{P}) = \{z_1, ..., z_{end}\}$ $\leftarrow$ Parameters

---

Output: $\mathcal{Y} = f_{\mathcal{Y}}(\mathcal{L}, \mathcal{Z}) = \{y_1, ..., y_{end}\}$ $\leftarrow$ Power demands to construct the power profile, where:

6 $y_i = \{P_{D,i}, P_{aux,i}, P_{tot,i}\}$ $\leftarrow$ Propulsion power, auxiliary power, and total power at point i

7 $P_{aux,i} = P_{aux,c}(X_v) + \Delta P_{aux,i}(O_{m,i}, T_{a,i}, X_v)$ $\leftarrow$ A constant auxiliary power demand based on the type of vessel, with fluctuations due to the operational modes and temperature

8 $P_{D,i} = \dfrac{f(s_{s,i}, w_{s,i}, c_{s,i}, h_i, w_{w,i}, f_{h,i}, \nabla_i) \cdot c_{0,i} \cdot V_{O_{m,i}}{}^a}{\eta_D}$

$\quad + |F_{tow,i}|^{\frac{3}{2}} \dfrac{2\pi K_Q}{\sqrt{\rho} D K_T^{\frac{3}{2}}}$ $\leftarrow$ This term is only applicable for tugboats and some OSVs

---

4 Modular control architecture

In this section, a modular control architecture is proposed, and a schematic view of the design is presented in Figure 7. The architecture is designed for the retrofittable power plant shown in Figure 4, and the control system consists of a supervisory level, a secondary level, and a primary level, and allows for modular use of the batteries in the power plant. In essence, the control architecture combines the concept of Supervisory Switching Control (SSC) (Hespanha, 2001; Hespanha and Morse, 2002; Nguyen et al., 2007) with Equivalent Consumption Minimization Strategy (ECMS) (Yuan et al., 2016; Kalikatzarakis et al., 2018). SSC has two characteristics; a supervisor and a bank of controllers. At any moment, the supervisor can decide to switch between the controllers in the bank, and in this paper, the supervisor switches based on the power profile for the mission, where each controller in the bank uses ECMS to determine the power split for the power plant equipment.

4.1 Supervisor

In this paper, we consider that only batteries can be added, replaced, or removed, and the main task of the supervisor is to determine the amount of batteries required for a given power profile, dictated by the mission. Due to the charging and discharging of the batteries during the mission, in this paper an upper bound for the required batteries ($P_{B,ub}$) will be defined. Therefore, it is assumed that the diesel generator set 2 is only used for emergencies,

and that the batteries are only discharged when the total electric power demand is higher than the optimal working point of diesel generator set 1 ($P_{DG,1}^{opt}$). Furthermore, the induction motor is used for propulsion, and only assisted by the diesel engine for high loads, and there are two available batteries for the power plant: type 1 and type 2, where the capacity of type 2 is twice the capacity of type 1. At last, each battery is charged to SOC_{max} at the beginning of the mission, such that:

$$P_{B,ub}(t) = max\left\{0,\ P_{aux}(t) + min\left\{P_{D,elec}(t), P_{IM,grid}^{max}\right\} - P_{DG,1}^{opt}\right\} \tag{25}$$

$$P_{D,elec}(t) = \frac{P_D(t)}{\eta_T \cdot \eta_{IM} \cdot \eta_{FC}} \tag{26}$$

$$P_{IM,grid}^{max} = \frac{P_{IM,mec}^{max}}{\eta_{IM} \cdot \eta_{FC}} \tag{27}$$

where $P_{IM,mec}^{max}$ and $P_{IM,grid}^{max}$ denote the maximum mechanical power output of the induction motor, and the corresponding electric input power required from the grid, respectively, $P_{D,elec}$ is the propulsion power in terms of electric power of the induction motor, and η_{FC} and η_{IM} are the efficiency of the frequency converter and the induction motor, respectively. The required battery capacity ($E_{B,plant}$) can be determined by integrating the found $P_{B,ub}$, and using the batteries SOC limits and a safety factor SF as follows:

$$E_{B,plant} = \frac{\int_{t=0}^{tm} P_{B,ub}(t)dt}{SOC_{max} - SOC_{min}} \cdot SF \tag{28}$$

with SF taking values between 1.1 - 1.2 (here 1.2), as often in literature extra battery capacity is installed. The configuration with the least amount of batteries that satisfies $E_{B,plant}$ is selected, and also the capacity of each battery $C_{0,1}$ and $C_{0,2}$ in ampere-seconds (As) is known such that the configuration can be found with Algorithm 2.

Algorithm 2: Determine Required Batteries for Mission

Input: Battery and Power Plant Specifics

1 K_{max} $\leftarrow$ Maximum number of batteries in the power plant
2 $E_{0,1}$ $\leftarrow$ Energy capacity of battery type 1 (J)
3 $C_{0,1}$ $\leftarrow$ Coulomb capacity of battery type 1 (As)
4 $E_{0,2}$ $\leftarrow$ Energy capacity of battery type 2 (J)
5 $C_{0,2}$ $\leftarrow$ Coulomb capacity of battery type 2 (As)
6 $E_{B,plant}$ $\leftarrow$ Required battery energy capacity (J)

---

7 $r_E = \dfrac{E_{0,2} - E_{0,1}}{E_{0,1}}$ $\leftarrow$ Express difference in capacity in terms of $E_{0,1}$
8 $\mathbf{E}_K = \text{zeros}(K_{max}, K_{max} + 1)$
9 **for** $i = 1 : K_{max}$ **do**
10   **for** $j = 1 : i + 1$ **do**
11       $E_K(i,j) = (j \cdot r_E + (i - r_E)) \cdot E_{0,1}$ $\leftarrow$ Compute capacity (J) of battery configurations
12   **end**
13 **end**
14 $[\boldsymbol{I}, \boldsymbol{J}] = \text{find}(\mathbf{E}_K >= E_{B,req})$ $\leftarrow$ Find indices of suitable configurations
15 $K_{plant} = min(\boldsymbol{I})$ $\leftarrow$ Select configuration with minimum of batteries
16 $J_{min} = min(\boldsymbol{J}(\boldsymbol{I}(:) == K_{plant}))$ $\leftarrow$ Select configuration closest to required capacity
17 $\boldsymbol{C}_0 = \text{ones}(1, K_{plant}) \cdot C_{0,1}$ $\leftarrow$ Fill configuration with battery type 1
18 **if** $J_{min} \geq 2$ **then**
19   **for** $j = 1 : J_{min} - 1$ **do**
20       $C_0(K_{plant} - j + 1) = C_{0,2}$ $\leftarrow$ Replace type 1 with type 2 if necessary
21   **end**
22 **end**

Output: Battery Configuration

23 K_{plant} $\leftarrow$ Amount of batteries in the power plant
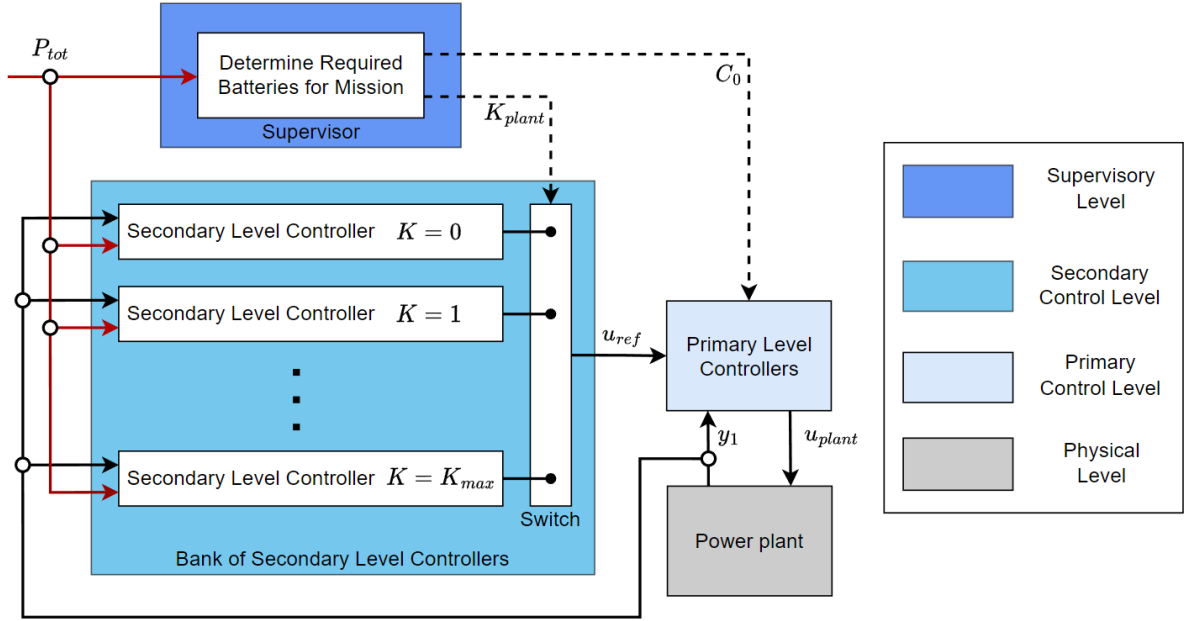24 $\boldsymbol{C}_0 \leftarrow$ Capacity of each battery

Figure 7: Modular power plant control architecture

4.2 Bank of secondary level controllers

The supervisor determines the required batteries for the power plant (K), while the rest of the equipment is fixed. As there is a certain physical limit of the number of batteries (K_{max}) in the power plant due to limited space, and if for example no batteries are required at all, the vessel also needs to be able to operate, thus resulting in $K \in \{0, 1, \cdots, K_{max}\}$. This leads to $K_{max} + 1$ different (possible) layouts for the power plant that can be represented as shown in Figure 7, where each secondary level controller in the bank uses ECMS to determine the power split for the installed equipment in the power plant. The next section discusses the required ECMS structure to find the power split for each layout, and the way this split is converted to reference-signals for the primary level.

4.3 ECMS and reference-signals

The secondary level control used for the modular control system consists of an ECMS with cost function and constraints, and a conversion of the power split to the reference signals. The cost function expresses the power of each component in terms of fuel use, while the constraints limit the power of each component to their capabilities, and ensure that the required power, as specified by the power profile, is met. Considering the modular use of multiple batteries, the optimization problem for the ECMS is structured as (Yuan et al., 2016; Kalikatzarakis et al., 2018):

$$minimize\{\dot{m}_{T,K}\} \tag{29}$$

where:

$$\dot{m}_{T,K} = a_1^{DE} \cdot P_{DE}^3 + a_2^{DE} \cdot P_{DE}^2 + a_3^{DE} \cdot \omega_{DE}^2 \cdot P_{DE} + a_4^{DE} \cdot \omega_{DE} \cdot P_{DE} + a_5^{DE} \cdot P_{DE}^2 \cdot \omega_{DE} + a_6^{DE} \cdot P_{DE}$$
$$+ \sum_{j=1}^{2} \left(a_1^{DG,j} \cdot \left(\frac{P_{DG,j}}{\eta_{DG,j}} \right)^3 + a_2^{DG,j} \cdot \left(\frac{P_{DG,j}}{\eta_{DG,j}} \right)^2 + a_3^{DG,j} \cdot \frac{P_{DG,j}}{\eta_{DG,j}} \right) \tag{30}$$
$$+ \sum_{k=1}^{K} \left(SFOC_{DE,nom} \cdot \eta_{FC} \cdot \eta_{IM} \cdot \eta_{B,k}^{sign(P_{B,k})} \cdot P_{B,k} \right)$$

subject to:

$$P_{DE} \geq \frac{P_D}{\eta_T} - P_{IM,mec} \tag{31}$$

$$\sum_{j=1}^{2} P_{DG,j} \geq P_{aux} - \sum_{k=1}^{K} P_{B,k} + \frac{P_{IM,mec}}{\eta_{IM} \cdot \eta_{FC}} \tag{32}$$

$$0 \leq P_{DE} \leq P_{DE}^{max} \tag{33}$$

$$0 \leq P_{IM,mec} \leq P_{IM,mec}^{max} \tag{34}$$

$$0 \leq P_{DG,j} \leq P_{DG,j}^{max} \qquad \text{for } j \in [1,2] \qquad (35)$$

$$P_{B,k}^{min} \leq P_{B,k} \leq P_{B,k}^{max} \qquad \text{for } k \in [1,...,K] \qquad (36)$$

$$P_{B,k} \geq P_{B,k-1} \qquad \text{for } k \in [2,...,K] \qquad (37)$$

$$P_{B,K} \cdot P_{B,1} \geq 0 \qquad \text{for } K \geq 2 \qquad (38)$$

Here, $\dot{m}_{T,K}$ is the fuel consumption rate for a power plant with K batteries in [kg/sec], $P_{DE}, P_{IM,mec}, P_{DG,j}$, and $P_{B,k}$ denote the power split regarding the diesel engine, induction motor, diesel generator set $j \in [1,2]$, and battery $k \in [1,...K]$, respectively, with limits $P_{DE}^{max}, P_{IM,mec}^{max}, P_{DG,j}^{max}, P_{B,k}^{min}$, and $P_{B,k}^{max}$. Furthermore, a_i^{DE} for $i = [1,2,3,4,5,6]$, $a_i^{DG,j}$ for $i = [1,2,3]$ are constants to characterize the fuel consumption, $SFOC_{DE,nom}$ is the nominal diesel engine fuel consumption, $\eta_{B,k}$ is the efficiency of battery k, and $\eta_{DG,j}$ the j-th diesel generator sets efficiency.

Remark: Note that the state-of-the-art methods for ECMS (Yuan et al., 2016; Kalikatzarakis et al., 2018) consider Equation 29 to 36 for $K = 1$. However, as this paper considers multiple batteries, constraint 37 which ensures each next battery produces equal or more power than the previous, and constraint 38 which ensures the batteries are either all charging or discharging, are included.

Using the above optimization problem for the ECMS, the power for each component is found, at each moment during the mission. This can be used to derive the following reference signals for the primary level: rotor speed for the induction motor $\omega_{IM,ref}$, torque of the diesel engine $Q_{DE,ref}$, voltage and shaft speed of diesel generator set $V_{DG,j,ref}$ and $\omega_{DG,j,ref}$, respectively for $j \in [1,2]$, and the reference power of the K batteries, $P_{B,k,ref}$.

$$\omega_{IM,ref} = i_{IM} \cdot \sqrt[3]{\frac{P_D}{C_p}} \qquad (39)$$

$$Q_{DE,ref} = \frac{P_{DE}}{\omega_{IM,ref}} \cdot \frac{i_{IM}}{i_{DE}} \qquad (40)$$

$$V_{DG,j,ref} = V_{grid} \qquad (41)$$

$$\omega_{DG,j,ref} = f_{grid} \cdot \frac{4\pi}{p_{DG,j}} \qquad (42)$$

where C_p is the propeller constant, i_{IM} and i_{DE} the induction motor and diesel engine gear ratios, V_{grid} and f_{grid} the required grid voltage and frequency, and $p_{DG,j}$ the number of poles of generator j.

5 Simulation results

This paper aims to investigate the behaviour of the modular power plant control architecture when used for a tugboat such as the Smith Elbe (Kalikatzarakis et al., 2018). A typical mission for a tugboat consists of: (i) *Transit* to the arrival location of the cargo vessel to be towed, (ii) remain *standby* at position until the cargo vessel arrives, (iii) *assist-low*, (iv) *assist-high*, in order to guide the cargo vessel into the harbour, and (v) *transit* back to a specific location in the harbour when finished. Each operational mode dictates a certain power demand, but also the operational environment and the time spend in each mode has an impact. To this end, four missions are composed, where for the baseline, mission 1, the power profile found in (Yuan et al., 2016) is considered. As
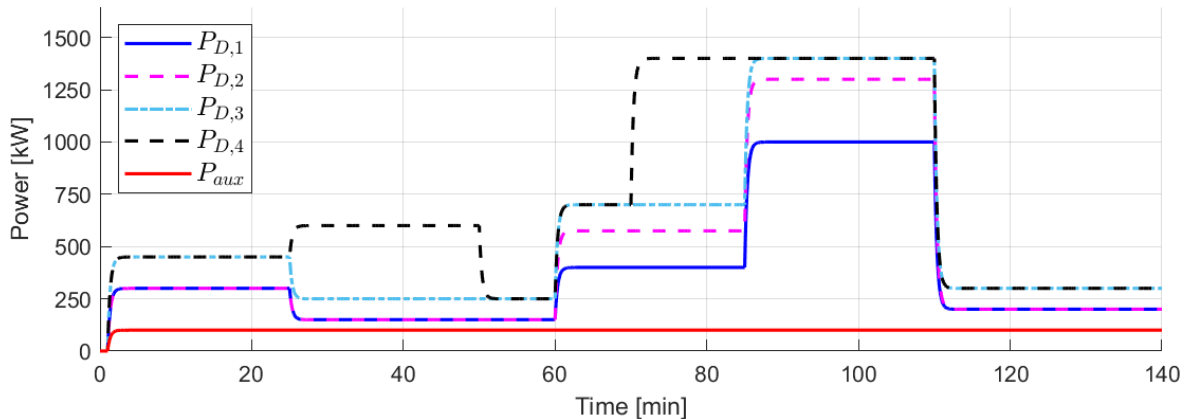

Figure 8: Power profiles of different scenarios

mission 2, 3, and 4 are all variations on mission 1, the described correlation between the mission and the power profile can be used to indicate changes in the power profile, based on the changes in the mission, and this is shown in Table 1. Note that only the propulsion power is affected, and for the auxiliary power a constant load of 100 kW is assumed for each mission.

	Change with respect to mission 1	Change with respect to power profile 1			
		Transit	Standby	Assit-low	Assist-high
Mission 1	-	-	-	-	-
Mission 2	Larger cargo ship to assist	-	-	Increase of F_{tow} $\rightarrow$ P_D increases	Increase of F_{tow} $\rightarrow$ P_D increases
Mission 3	Larger cargo ship to assist	-	-	Increase of F_{tow} $\rightarrow$ P_D increases	Increase of F_{tow} $\rightarrow$ P_D increases
	Increase of wave, wind, and currents	Increase of s_s, w_s, c_s $\rightarrow$ P_D increases	Increase of s_s, w_s, c_s $\rightarrow$ P_D increases	Increase of s_s, w_s, c_s $\rightarrow$ P_D increases	Increase of s_s, w_s, c_s $\rightarrow$ P_D increases
Mission 4	Larger cargo ship to assist	-	-	Increase of F_{tow} $\rightarrow$ P_D increases	Increase of F_{tow} $\rightarrow$ P_D increases
	Increase of wave, wind, and currents	Increase of s_s, w_s, c_s $\rightarrow$ P_D increases	Increase of s_s, w_s, c_s $\rightarrow$ P_D increases	Increase of s_s, w_s, c_s $\rightarrow$ P_D increases	Increase of s_s, w_s, c_s $\rightarrow$ P_D increases
	Cargo ship arrives further from starting point of tugboat, but total mission time remains the same	Longer duration of mode* / Speed increase halfway during mode* $\rightarrow$ P_D increases*	Shorter duration of mode	Shorter duration of mode	Longer duration of mode

Table 1: Changes in mission and power profile. *: Only applies for the first use of this mode. For the second use of this mode, the arriving point of the cargo vessel is not important.

The described variation in the mission and the power profile, as shown in Table 1, are used to construct the four different power profiles shown in Figure 8. For each mission, at $t = 0$ the supervisor determines the required batteries for the mission, selects the corresponding secondary level controller from the bank, automatically initializes the primary level battery constraint modules, and also selects the required battery models in the power plant model, and in Table 2 the required batteries and their capacity for each mission can be found. During the simulations, the behavior of the secondary and primary level, and also of the power plant components is monitored. The parameters used for the simulations are shown in Table 4, and the simulation results are presented in Figure 9. In Figure 9a, 9d, 9g, and 9j the power split for the fixed equipment can be seen, in Figure 9b, 9e, 9h, and 9k the power split for the batteries is shown, and in Figure 9c, 9f, 9i, and 9l the batteries SOC levels are presented. Note that the power split is provided by the secondary level, while the SOC levels are given by the battery constraint modules in the primary level. From the results it can be seen that the modular control architecture performs well for each mission, as the power split for all the components is stable, and the SOC of the batteries is kept within its limits. The robustness of the modular control architecture follows from the stable behavior for both different power profiles and different power plant layouts. Furthermore, using the generated power split and the SOC of the batteries, it can be noted

	$E_{B,max}$	K	Type	Selected Batteries			
				Capacity			
				E_0		C_0	
Mission 1	904 MJ	1	2	1080	MJ	2.4	MAs
Mission 2	1294 MJ	2	[1,2]	[540 1080]	MJ	[1.2 2.4]	MAs
Mission 3	1625 MJ	2	[2,2]	[1080 1080]	MJ	[2.4 2.4]	MAs
Mission 4	2404 MJ	3	[1,2,2]	[540 1080 1080]	MJ	[1.2 2.4 2.4]	MAs

Table 2: Supervisor results for different missions

that either the battery power or the SOC behaves proportional to the ratio of the batteries' capacities. As observed in Figure 9e and 9f, where a battery of type 2 shows similar SOC decrease for a discharging power twice as much as for a battery of type 1. Even more, for the same charging rate, a battery of type 1 charges much faster than a battery of type 2, as it has a smaller capacity. At last, it can be noted that although batteries in the power plant have the same capacity, the secondary level could decide to discharge or charge them with different rates, as can be seen in Figure 9h and 9k.

In order to give quantitative results, for each mission the measured output of the power plant components is used to determine the delivered propulsion $P_{D,plant}$ and auxiliary power $P_{aux,plant}$, as shown in Equation 43 and 44.

$$P_{D,plant} = Q_p \cdot \omega_p \tag{43}$$

$$P_{aux,plant} = \sum_{j=1}^{2} V_{DG,j} \cdot I_{DG,j}^* + \sum_{k=1}^{K} V_{B,k} \cdot I_{B,k} - \frac{Q_{IM} \cdot \omega_{IM}}{\eta_{IM} \cdot \eta_{FC}} \tag{44}$$

where * denotes the complex conjugate. Using this, the RMSE and the scatter index (SI) with respect to the requested propulsion P_D and auxiliary power P_{aux}, as stated by the power profile, can be determined using Equation 45, and the results are presented in Table 3. It can be seen that with respect to the tracking of the propulsion power, the control system performs quite well (SI < 3%), and also the tracking of the auxiliary power is quite good (SI < 11%). Furthermore, it can be noted that the more demanding a mission, the smaller the propulsion tracking errors get, while the auxiliary power tracking seems to increase a little.

$$\text{Power error} \begin{cases} \text{RMSE} & = \sqrt{\text{mean}\left(\left(P_i - P_{i,plant}\right)^2\right)} \\ \text{SI} & = \dfrac{\text{RMSE}}{\text{mean}(P_{i,plant})} \end{cases} \quad \text{for } i \in \{'D','aux'\} \tag{45}$$

	Propulsion Power Error		Auxiliary Power Error	
	RMSE [kW]	SI [%]	RMSE [kW]	SI [%]
Mission 1	9.12	2.39	10.43	10.55
Mission 2	10.88	2.34	10.02	10.15
Mission 3	10.99	1.90	10.54	10.68
Mission 4	11.27	1.58	10.50	10.64

Table 3: Performance of modular power plant controller

Induction Motor			**Batteries**			**Diesel Engine**			**Diesel Generator Sets**		
Model Parameters			*Model Parameters*			*Model Parameters*			*Model Parameters*		
k_{DE}	1000	$\frac{m}{s^2}$	$SOC(t_0)$	1	[-]	k_{DE}	3000	$\frac{m}{s^2}$	k_{DG}	4000	$\frac{m}{s^2}$
R_2	0.01	Ω	$a_{B,1}$	111	V				J_{DG}	4167	kgm^2
			$a_{B,0}$	389	V				$R_{DG,int}$	0.150	Ω
			R_B	0.0225	Ω				L_{DG}	0.0021	H
									$a_{G,1}$	3.34	$\frac{s^4}{kgm^2}$
Controller Gains			*Constraint Module Parameters*			*Controller Gains*			$a_{G,0}$	0.57	$\frac{As^4}{kgm^2}$
$K_{P,IM}$	10	[-]	Δt	1000	s	$K_{P,DE}$	20	[-]			
$K_{I,IM}$	10	[-]	$SOC_{B,min}$	0.1	[-]	$K_{I,DE}$	2	[-]	*Controller Gains*		
$C_{V/f}$	2	$\frac{s}{Nm}$	$SOC_{B,max}$	1	[-]				$K_{P,DG,DE}$	200	[-]
			$V_{B,min}$	300	V	*ECMS Parameters*			$K_{I,DG,DE}$	30	[-]
ECMS Parameters			$V_{B,max}$	600	V	a_1^{DE}	$5.48 \cdot 10^{-5}$	$\frac{kg}{GW^3h}$	$K_{P,DG,G}$	30	[-]
η_{IM}	0.95	[-]				a_2^{DE}	-0.206	$\frac{kg}{MW^2h}$	$K_{I,DG,G}$	12	[-]
P_{IM}^{max}	$800 \cdot 10^3$	W	*ECMS Parameters*			a_3^{DE}	$5.545 \cdot 10^{-4}$	$\frac{kgs^2}{kWh}$			
			η_B	0.97	[-]	a_4^{DE}	-0.271	$\frac{kgs}{kWh}$	*ECMS Parameters*		
			$SFOC_{DE,nom}$	72.1	$\frac{kg}{kWh}$	a_5^{DE}	$-3.55 \cdot 10^{-5}$	$\frac{kgs}{MW^2h}$	a_1^{DG}	$5.55 \cdot 10^{-4}$	$\frac{kg}{GW^3h}$
Shaft and Gearbox						a_6^{DE}	600	$\frac{kg}{kWh}$	a_1^{DG}	-0.580	$\frac{kg}{MW^2h}$
J_{tot}	12500	kgm^2	**Electric Grid**			P_{DE}^{max}	$1200 \cdot 10^3$	W	a_3^{DG}	$2.15 \cdot 10^2$	$\frac{kg}{kWh}$
i_{DE}	7.5	[-]	V_{grid}	3300	V				η_{DG}	0.95	[-]
i_{IM}	24	[-]	f_{grid}	50	$\frac{1}{s}$	**Propeller**			P_{DG}^{max}	$665 \cdot 10^3$	W
η_T	0.95	[-]	η_{FC}	0.99	[-]	C_p	670	kgm^2	P_{DG}^{opt}	$524 \cdot 10^3$	W

Table 4: Parameters of the power plant components

(a) Mission 1: Fixed equipment power   (b) Mission 1: Battery power   (c) Mission 1: Battery SOC

(d) Mission 2: Fixed equipment power   (e) Mission 2: Battery power   (f) Mission 2: Battery SOC

(g) Mission 3: Fixed equipment power   (h) Mission 3: Battery power   (i) Mission 3: Battery SOC

(j) Mission 4: Fixed equipment power   (k) Mission 4: Battery power   (l) Mission 4: Battery SOC
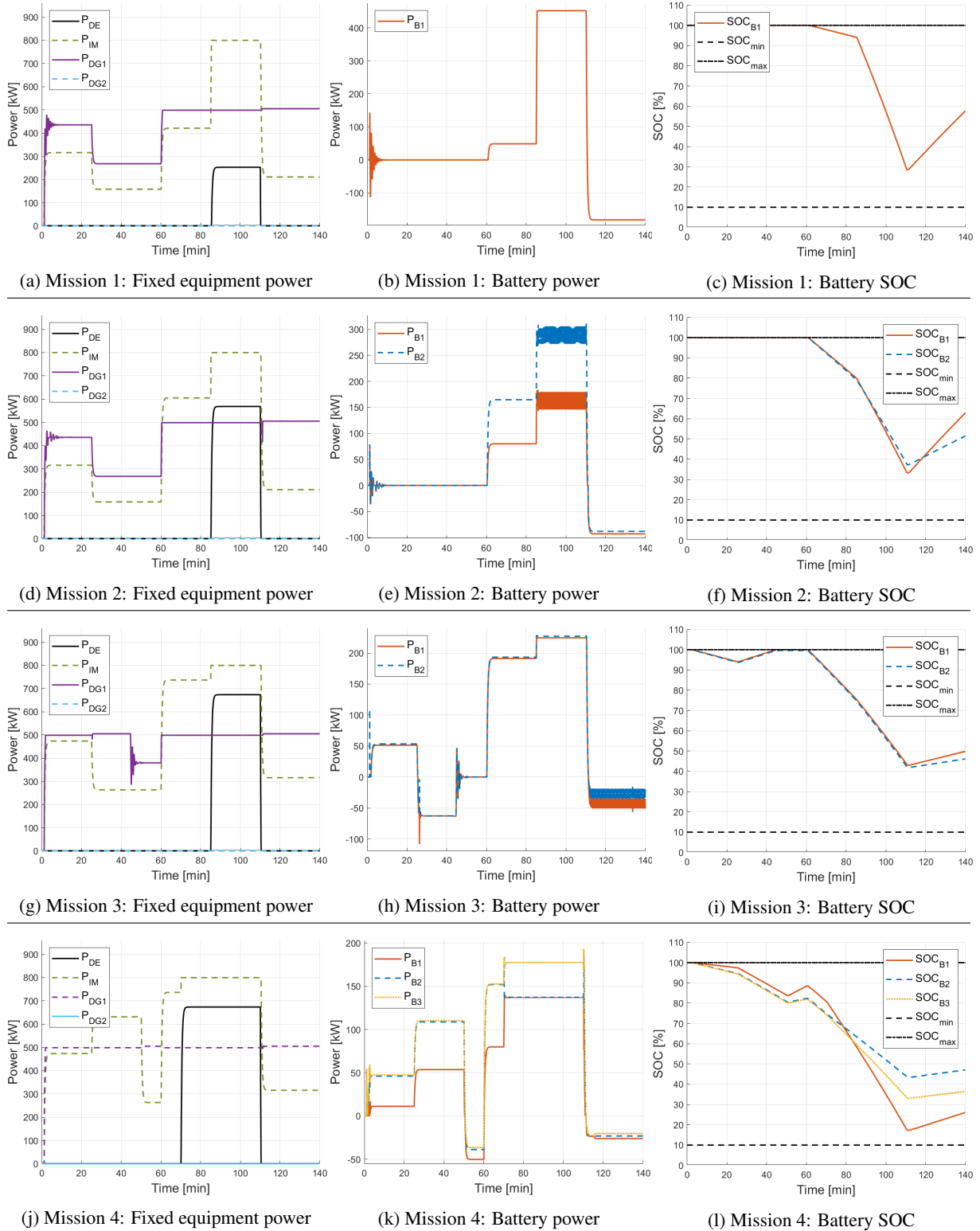
Figure 9: Simulation results

6 Conclusions

In this paper, a graph-model for the correlation between the mission and the power profile is presented, and the correlation between the power profile and the automation modifications of the control system is discussed. Using this, a modular control architecture for a retrofittable power plant is proposed, which allows modular use of the batteries. Simulations showed the performance of the modular control architecture, regarding the stability and robustness. The results indicate a tracking error of the propulsion and auxiliary power requested by the power profile for four missions with different characteristics to be less than 3% and 11% (as shown in Table 3), respectively.

Acknowledgement

References

Chang, W., 2013. The state of charge estimating methods for battery: A review. International Scholarly Research Notices 2013.

Cheong, K., Li, P., Xia, J., 2010. Control oriented modeling and system identification of a diesel generator set (genset), in: Proceedings of the 2010 American Control Conference, IEEE. pp. 950–955.

Eijkhout, T., Jovanova, J., 2021. Active heave compensation of a floating crane using electric drive, in: 2021 IEEE/ASME International Conference on Advanced Intelligent Mechatronics (AIM), pp. 1089–1094. doi:10.1109/AIM46487.2021.9517502.

Geertsma, R., 2019. Autonomous control for adaptive ships: with hybrid propulsion and power generation. Ph.D. thesis. Delft University of Technology.

Geertsma, R., Negenborn, R., Visser, K., Hopman, J., 2016. Torque control for diesel mechanical and hybrid propulsion for naval vessels, in: Proceedings of the 13th international naval engineering conference. Bristol, UK, pp. 476–92.

Geertsma, R., Negenborn, R., Visser, K., Hopman, J., 2017a. Design and control of hybrid power and propulsion systems for smart ships: A review of developments. Applied Energy 194, 30–54.

Geertsma, R., Negenborn, R., Visser, K., Loonstijn, M., Hopman, J., 2017b. Pitch control for ships with diesel mechanical and hybrid propulsion: Modelling, validation and performance quantification. Applied Energy 206, 1609–1631.

Geertsma, R.D. Negenborn, R., Visser, K., Hopman, J., 2017c. Parallel control for hybrid propulsion of multifunction ships. IFAC-PapersOnLine 50, 2296–2303.

Hanbidge, P., 2001. A mission-based approach to vessel design the royal institution of naval architects (rina) small craft safety. URL: https://www.academia.edu/14563968/A_MISSION_BASED_APPROACH_TO_VESSEL_DESIGN_The_Royal_Institution_of_Naval_Architects_RINA_SMALL_CRAFT_SAFETY.

Haseltalab, A., van Biert, L., Mestemaker, B., Negenborn, R., 2020. Energy Management for Hybrid Power Generation Using Solid Oxide Fuel Cell, Zenodo. URL: https://doi.org/10.24868/issn.2631-8741.2020.006, doi:10.24868/issn.2631-8741.2020.006.

Haseltalab, A., Negenborn, R., 2019. Model predictive maneuvering control and energy management for all-electric autonomous ships. Applied Energy 251, 113308.

Hespanha, J., 2001. Tutorial on supervisory control, in: Lecture Notes for the workshop Control using Logic and Switching for the 40th Conf. on Decision and Contr., Orlando, Florida, Citeseer.

Hespanha, J., Morse, A., 2002. Switching between stabilizing controllers. Automatica 38, 1905–1917.

Izadi-Zamanabadi, R., Blanke, M., 1999. A ship propulsion system as a benchmark for fault-tolerant control. Control Engineering Practice 7, 227–239.

Kalikatzarakis, M., , R., Boonen, E., Visser, K., Negenborn, R., 2018. Ship energy management for hybrid propulsion and power supply with shore charging. Control Engineering Practice 76, 133–154.

Kularatna, N., Gunawardane, K., 2021. Rechargeable battery technologies: An electronic circuit designer's viewpoint. pp. 65–98. doi:10.1016/B978-0-12-820778-9.00001-2.

Kumar, B., Selvaraj, R.and Desingu, K., Chelliah, T., Upadhyayula, R., 2020. A coordinated control strategy for a diesel-electric tugboat system for improved fuel economy. IEEE Transactions on Industry Applications 56, 5439–5451.

Milis, G., Panayiotou, C., Polycarpou, M., 2017. Semiotics: Semantically enhanced iot-enabled intelligent control systems. IEEE Internet of Things Journal 6, 1257–1266.

Nguyen, T.D., Sørensen, A.J., Quek, S.T., 2007. Design of hybrid controller for dynamic positioning from calm to extreme sea conditions. Automatica 43, 768–785.

Smogeli, Ø., 2006. Control of marine propellers: from normal to extreme conditions .

Smogeli, Ø., Ruth, E., Sorensen, A., 2005. Experimental validation of power and torque thruster control, in: Proceedings of the 2005 IEEE International Symposium on, Mediterrean Conference on Control and Automation Intelligent Control, 2005., IEEE. pp. 1506–1511.

Smogeli, Ø., Sørensen, A., 2009. Antispin thruster control for ships. IEEE transactions on control systems technology 17, 1362–1375.

Smogeli, Ø., Sørensen, A., Minsaas, K., 2008. The concept of anti-spin thruster control. Control Engineering Practice 16, 465–481.

Sun, K., Shu, Q., 2011. Overview of the types of battery models, in: Proceedings of the 30th Chinese Control Conference, IEEE. pp. 3644–3648.

Vahedpour, M., Noei, A., Kholerdi, H., 2015. Comparison between performance of conventional, fuzzy and fractional order pid controllers in practical speed control of induction motor, in: 2015 2nd International Conference on Knowledge-Based Engineering and Innovation (KBEI), IEEE. pp. 912–916.

Van Benten, M., 2021. Multi-level propulsion control in complex ships. URL: `https://zenodo.org/record/6815283`.

Van Benten, M., 2022. Mission-oriented modular control of retrofittable marine power plants. URL: `https://repository.tudelft.nl/islandora/object/uuid:c48bd63b-b203-4cd3-ab66-2a63d315ef3a?collection=education`.

Vu, T., Ayu, A., Dhupia, J., Kennedy, L., Adnanes, A., 2015. Power management for electric tugboats through operating load estimation. IEEE Transactions on Control Systems Technology 23, 2375–2382.

Wang, S., Wang, L., Qiao, Z., Li, F., 2018. Optimal robust control of path following and rudder roll reduction for a container ship in heavy waves. Applied Sciences 8, 1631.

Wildi, T., et al., 2002. Electrical machines, drives, and power systems. New Jersey: Upper Saddle River .

Woud, H.K., Stapersma, D., 2019. Design of propulsion and electric power generation systems. IMarEST, Institute of Marine Engineering, Science and Technology.

Yuan, L., Tjahjowidodo, T., Lee, G., Chan, R., dnanes, A.K., 2016. Equivalent consumption minimization strategy for hybrid all-electric tugboats to optimize fuel savings, in: 2016 American Control Conference (ACC), IEEE. pp. 6803–6808.